Chapter 2
Experiment Approaches and Simulation Methods

2.1 Synthesis and Characterization of Graphene Specimen

In this section, firstly the preparation methods of graphene samples were introduced, including the synthesis of monolayer and multilayered graphene by CVD, substrate etching and graphene transfer. Secondly, the main characterization methods of graphene before and after processing were introduced. Finally, the equipment for processing of graphene by particle beam irradiation was introduced.

2.1.1 Preparation of Monolayer and Multilayer Graphene Specimens

2.1.1.1 CVD Preparation Method

The graphene was synthesized by CVD method. For the preparation of multi-layer graphene, the name and model of the equipment used in this paper is tube resistance furnace GERO F100-750/13 with a furnace size 350 × 950 × 420 mm, and furnace cavity diameter Ø100 mm. The maximum temperature can reach 1300 °C. Figure 2.1 shows a schematic diagram of the CVD setup for the preparation of graphene.

The CVD method for the preparation of graphene films mainly involves the following steps:

(1) Cleaning of the heating pipe. Use a volatile liquid (alcohol) to clean the pipe in the tube.
(2) Selection of growth substrate. In order to grow monolayer and a few layers of graphene samples, the substrates on which graphene grows were selected as Pt and Cu, respectively. The growth of graphene on the Pt substrate depends on the dissolution of the carbon atoms in the carbon atmosphere at high

© Springer Nature Singapore Pte Ltd. 2018

X. Wu, *Influence of Particle Beam Irradiation on the Structure and Properties of Graphene*, Springer Theses, https://doi.org/10.1007/978-981-10-6457-9_2

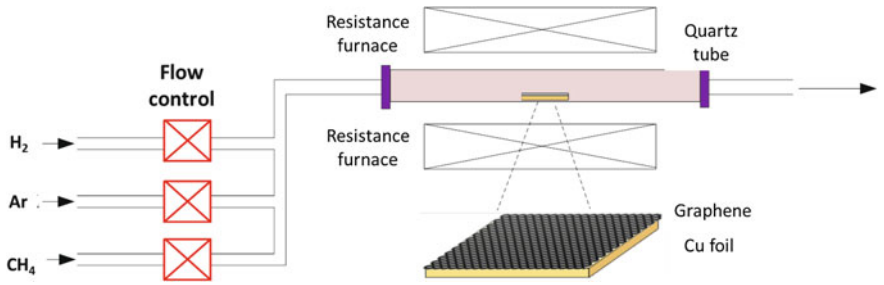


Fig. 2.1 Schematic diagram of the CVD apparatus for the preparation of graphene

temperature and crystallization at low temperature. The Cu-based growth graphene is directly crystallized on the surface by the deposited carbon atoms. Due to the limitation of the growth environment, the few layers graphene was grown by Cu substrate, and the monolayer graphene film was grown by Pt substrate. Most of the experiments used few layers graphene samples. Therefore, only the growth of graphene on Cu substrate was introduced in detail. The copper foil was manufactured by Alfa Aesar and has a mass purity of 99.8% and a thickness of 25 μm. Before the experiment, the copper foil was pre-cleaned by ultrasonic and cut into the appropriate size.

(3) Sealing and pumping the protective gas. The copper foil was placed at constant temperature area of the tube furnace, and then sealed tube furnace. Then the argon was pumped in, and sealing results were checked to strictly guarantee the gas seal.

(4) Hydrogen input. Set the program for heating with a heating rate of 10 °C/s. When the furnace temperature rose to 400 °C, the hydrogen could be pumped in with a gas flow as shown in Table 2.1.

(5) Carbon source input. When the temperature rose to 1000 °C, the gas flow of argon and hydrogen was adjusted, and this temperature was kept for 60 min. Afterwards, carbon source (methane) began to be inputted in.

(6) High temperature reaction. Methane gas began to decompose under the reduction of hydrogen for about 10 min. The furnace temperature during the reaction was 1000 °C. After the completion of the reaction, we stopped the methane, and moved the copper foil to low temperature area of the furnace.

(7) Sample cooling. Turn off the hydrogen and resistance furnace power supply so that the sample was cooled to room temperature with argon.

Table 2.1 Gas flow at different stages of graphene preparation by CVD method

Gas	Heating (mL/min)	Growth (mL/min)	Air cooling (mL/min)	Final (mL/min)
Ar	0.7	1.6	0.5	0
H_2	400	400	0	0
CH_4	0	30	0	0

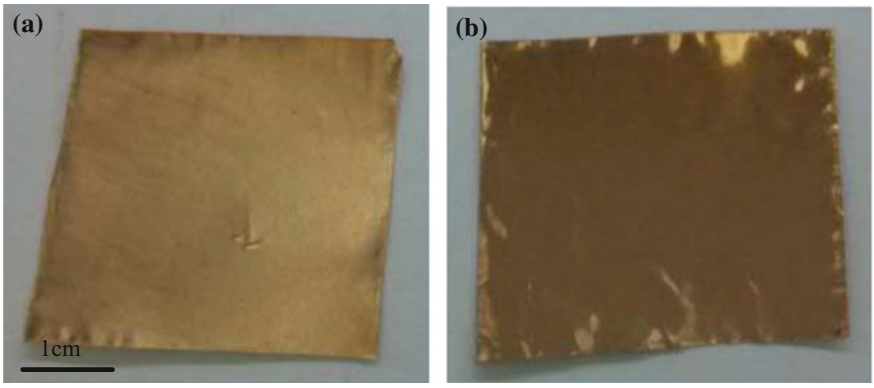


Fig. 2.2 Appearance of copper substrate **a** before and **b** after growth of graphene

(8) Samples taken out. Remove the sample from the furnace and store it in a suitable environment. Then the laboratory equipment was recovered.

The final graphene sample prepared on the copper substrate is shown in Fig. 2.2. The copper base is bright yellow before growth of graphene and becomes dark yellow after growth of graphene.

2.1.1.2 Substrate Etching and Graphene Transfer

The transfer of the substrate mainly involves the etching of the growth substrate and the reloading of the target substrate. For the graphene grown on Pt substrate, the surface PMMA was used to help with the etching. PMMA can ensure the quality of monolayer graphene film, but the subsequent removal process is complicated. For the graphene grown on the copper foil substrate, the $FeCl_3$ solution was directly used to etch the substrate. Because the strength of graphene film is high, it can be transferred to the target substrate quickly and easily.

The transfer of graphene was divided into the following steps: (1) cutting the wafer and cleaning. The silicon wafer used for the experiment is a 4-in. single-side polished monocrystalline silicon with 300 nm thickness oxide layer. The thickness of the wafer is 360 μm. (2) Preparation of the etchant. Corrosive solution was made up by the mixed solution of 0.5 mol/L ferric chloride and 0.5 mol/L hydrochloric acid. (3) Etching of copper substrate. The copper-supported graphene was placed in the culture dish for etching for about 60 min. (4) Cleaning by deionized water. After the completion of the etching, the floating graphene was taken out and placed in deionized water for about 60 min, and the process was repeated 3–4 times until the graphene was perfectly cleaned. (5) Transferring to the target substrate. The graphene film was taken out from deionized water by using the silicon wafer. At this time, the graphene was transferred from the initial substrate to the target substrate. (6) Characterization of the samples. The samples were characterized with a microscope to evaluate the quality. Figure 2.3 shows the transferred graphene on the silicon substrate.

2.1.2 The Main Characterization Methods of Graphene Sample

The characterization of the structural morphology and performance of graphene samples before and after processed by particle beam irradiation needs a variety of modern microscopic analysis techniques to be used. Different analytical methods can be used to characterize graphene from different perspectives. The main characterization methods used in this paper are presented below.

(1) Optical microscopy

Optical microscope is a preliminary method of characterizing the microstructure of the material. Due to the substrate and the graphene structure reflect differently to the incident light, the graphene film on the silica substrate has a special color, which makes the structure of the graphene be resolvable and distinguishable. In this paper, the model of the optical microscope equipment is OLYMPUS BX51M, The amplification ranges from 50 to 1000 times.

(2) Scanning electron microscopy

SEM can be used to observe the microstructure of graphene, the surface morphology of the substrate, and the structural changes before and after graphene processing. In this paper, the SEM device is LEO-1530, with a resolution of 1 nm, and magnification of 20–900,000 times. The accelerating voltage of the electron beam is 100 V–30 kV.

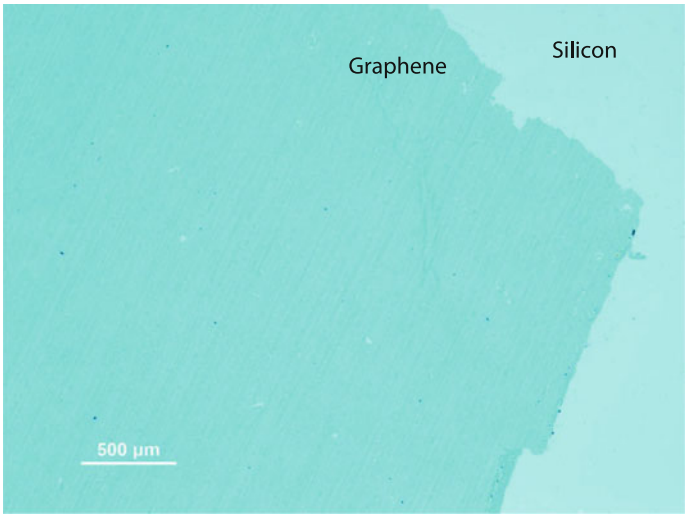


Fig. 2.3 Graphene on a silicon substrate

(3) High resolution transmission electron microscopy

TEM was used to process the graphene nanopore structure. The structure information of graphene and the number of layers of graphene and graphene edge morphology can also be observed by TEM. The model is Tecnai G2 F20 S-Twin. The maximum acceleration voltage is 200 kV with a point resolution of 0.24 nm, and the minimum beam spot size is 0.3 nm.

(4) Raman spectroscopy

Raman spectroscope is widely used in the characterization of carbon materials [1]. The graphene usually has three main characteristic peaks, namely, the D peak caused by defects near 1350 cm^{-1}, the G peak caused by E_{2g} vibration near 1584 cm^{-1}, and the overtone peak 2D peak near 2680 cm^{-1}. D peak represents the defects in the structure of graphene, which can reflect the damage of graphene structure before and after processing in graphene doping and nanopore fabrication. The peak intensity ratio and position information of G peak and 2D peak can reflect the layer information of graphene. Usually, the 2D peak of single layer graphene is stronger than G peak. If the overlapped graphene is joined with each other, the intensity of 2D peak will decrease gradually when the number of layers increases, and the location will shift right as well. Therefore, the joining between graphene layers can be determined by analyzing the peak intensity ratio of the G peak and the 2D peak. The mode of Raman analysis equipment is LabRAM HR Evolution. The laser spot used was 1.25 μm, and the analysis band was 1000–3500 cm^{-1}. The acquisition time was 20 s, and the power of the laser was 0.38 mW. In addition, Raman Imaging was used to analyze the changes of graphene structure in the processing area in batch, and the uniformity of the results was also analyzed.

(5) Atomic force microscopy

AFM can analyze the surface fluctuation of graphene from the atomic level, and the changes of graphene structure before and after irradiation by particle beam. Through the contact mode, the height information of graphene at the boundary before and after joining can be analyzed, which can be used to decide whether joint is formed or not. In addition, by analyzing the morphological information of the nanopore structure, it is possible to describe the size, depth and three-dimensional structure information. The device model is Veeco USA.

(6) X-ray photoelectron spectroscopy

The XPS can analyze the composition and structure of the surface elements of the graphene films. The doping information of the graphene structure and the chemical bonding formed between the elements can be obtained by the analysis of the peak fitting of the chemical elements. XPS analysis equipment model is ESCALA8 250 Xi, and the best energy resolution is less than 0.45 eV.

2.1.3 The Main Experimental Equipment for Graphene Processing

1. SEM/FIB double beam system

For the processing of nanopore and nanoribbon in supported single layer graphene, a SEM/FIB double beam system was used in this paper. Among them, the FIB was used to process the graphene nanostructures, and the SEM was used to observe the processing in situ. The focal ion source used in the apparatus was gallium ion, and the ion beam energy was fixed at 30 keV. The ion beam was focused into a beam spot with a diameter of about 5 nm using a focusing system. By selecting different ion beam streams, and controlling the moving speed of the workbench, different levels of micro-etching can be achieved for the sample. SEM used the field emission filament. In order to reduce the destruction of the electron beam on the sample, an electron beam acceleration voltage of 5 kV was adopted, and the electronic current was 1 pA. The equipment was manufactured by TESCAN (Czech), and model is LYRA 3 FEG.

2. Low energy ion implantation machine

The experimental equipment used for low energy ion implantation is a plasma immersion ion implantation machine, which utilizes an inductive coupling to produce a high-density plasma in a reaction chamber by a set of high-power radio frequency excitation power sources. In the meantime, another group of pulsed bias power sources directs ions perpendicularly move to the sample, which could inject the ions into the interior of the sample. This system can realize the purpose of high dose low energy injection with low damage. The gas flow rate of the ion implantation process was 250 mL/min, and the power was set as 800 w, with a pulse width of 30 μs. The energy of the implanted ions and the injection time were controlled to realize the injection of ions with different energy and dose. The excitation power was 13.56 MHz and 1500 W, with an injection bias of 0–5 kV. The equipment model is PIII-200.

3. Femtosecond laser system

The laser-processing of micron structure on graphene used COHERENT Company's semiconductor pump-mode injection molding titanium sapphire laser amplifier. The laser center wavelength was 800 nm, and the pulse width was 50 fs, with a maximum repetition frequency of 1000 Hz, and the focused spot of the laser after focusing through the lens was about 10 μm. The initial output power of the femtosecond laser was 3.52 W, and the laser power was controlled by two-stage attenuation method, so as to study the processing damage of the graphene structure under different energy laser.

2.2 Introduction of MD Simulation

2.2.1 Concepts

MD simulation is an important method in computational materials science. MD mainly refers to that according to the initial conditions of the system in the ground state, the use of computer simulations to integrally solve the motion state of the system under the external conditions, based on the empirical or semi-empirical parameters. Through averaging of the molecular microscopic state in the time and space, we can get the macro physical quantities of the system, such as the system temperature, pressure, energy and so on. It can also get the structural information of the system in equilibrium state. MD simulation is divided into the first-principle MD simulation based on quantum mechanics and classical MD simulation based on Newton's second law. Among them, the classic MD can solve a system with tens of thousands of atoms on an ordinary computer, and it can also investigate the phenomenon and mechanism of graphene processed by particle beam irradiation from atomic scale level. In this article, if it is not specifically described, the MD particularly refers to the classical MD simulation.

2.2.2 Basic Principles of Classic MD

Classical MD refers to the using of computer simulation to get the structure and properties of a system made up of nuclei and nuclear electrons. The movement of each nucleus follows Newton's law of motion and the nucleus is considered to move under the average potential of all other nuclei and electrons. For the interaction of nuclei-nuclei, nuclei-electron, and electron-electron, analytical potential is adopted. Classic MD is generally divided into the following steps:

1. Determination of the research model. Extracting the corresponding physical model according to the problem to be studied, and then establishing the corresponding MD model.
2. Selection of the force field. Selecting the appropriate force field to describe the interatomic interaction potential energy and determining the parameters of the force field.
3. Boundary conditions. The supercell of MD simulation is only a repeating unit of the macro system. In order to simulate the free system or periodic system, it is needed to set a fixed, shrink wrap or periodic boundary conditions.
4. System initialization. Calculating the minimum energy of the system with a given initial conditions to get the steady-state structure of the system under initial equilibrium conditions, which could provide the equilibrium structure for the following dynamics simulation under the external conditions.

5. Solution of Newton equation. Under the external conditions, the force and potential energy of the particles in the system are solved and the iterations are repeated until the requirements are satisfied.
6. Output of the results, averaging of macro physical quantity.

It can be seen from the simulation process that the selection of the interaction potential between atoms is very important for the simulation results of graphene materials. The choice of numerical integration algorithm, the simulation system ensemble and the results statistical method have great influence on the accuracy of the results. They will be described in detail in next section.

2.2.3 Atomic Interaction Force

The key to the classical MD simulation lies in the selection of the potential energy function for the interaction between atoms. Because of the complexity of the simulation system and the different interactions between different elements, it is difficult to describe the interaction between different simulation systems and different elements by using a unified potential energy function. In the actual simulation process, it is often necessary to select the appropriate potential function according to the change of the simulation system and the composition of the atomic structure. In this paper, AIREBO [2] was used to describe the interaction between graphene carbon atoms, and L-J potential was used to describe the interaction between carbon atoms in graphene and Si, O atoms in substrate. ZBL [3] potential was selected to describe the collision between the incident ions and the target atoms, and Tersoff [4] potential was adapted to describe the interaction between N, B and C atoms, and also the interaction between Si and O atoms.

2.2.3.1 L-J Potential

The interaction between the carbon atoms in graphene and the Si, O atoms in the silica substrate was described by van der Waals forces. In addition, the carbon atoms in the graphene also exist a van der Waals force between molecules in long-range. In this study, the general 12/6 potential energy form was selected to describe the van der Waals force between different atoms in the simulation system, in which the substrate and graphene were generally considered as electrostatic balance system. Thus the intermolecular Coulomb's potential contact was ignored. The van der Waals intermolecular force was expressed as:

$$E_{ij}^{LJ} = 4\varepsilon\left[\left(\frac{\sigma_{ij}}{r}\right)^{12} - \left(\frac{\sigma_{ij}}{r}\right)^{6}\right] \quad r < r_c \tag{2.1}$$

In Eq. (2.1), ε is the energy parameter and σ is the distance parameter.

In order to save the simulation time, it is generally necessary to set a cutoff distance r_c for the force, and the interaction between the atoms outside the cutoff distance is very weak and negligible. Specific calculation parameters and cutoff radius will be introduced for different models in subsequent simulations.

2.2.3.2 AIREBO Potential

For the interaction between carbon atoms in graphene, the AIREBO was selected. This potential energy function can accurately describe the combination of strong hybrid bonds of sp, sp^2, sp^3 in graphene and the conversion between different hybrid bonds. Meanwhile, it can also accurately describe the brokenness of old chemical bonds and formation of new bonds in the process of graphene joining, doping and nanopore drilling. In addition, it is able to describe the bond energy, bond length, elastic properties, defect formation and surface energy changes during the process of structural transformation. This potential is based on the REBO potential from Brenner, and has been widely used in the study of properties and structure of carbon nanomaterials. The expression of this potential energy is:

$$E = \frac{1}{2}\sum_i \sum_{j \neq i} \left[E_{ij}^{REBO} + E_{ij}^{LJ} + \sum_{k \neq i,j} \sum_{l \neq i,j,k} E_{kijl}^{tor} \right] \tag{2.2}$$

The first term on the right side of (2.2) is the covalent bond (REBO) term, the second term is the intermolecular long-range action term (L-J), and the third term is the torsion item describing the bond rotation. The models in this paper only considered the first two items, for which L-J item was already mentioned in Sect. 2.2.3.1, REBO item can be expressed as:

$$E_{ij}^{REBO} = V_{ij}^R + b_{ij} V_{ij}^A \tag{2.3}$$

In which, V_{ij}^R and V_{ij}^A represent the exclusion and attraction items, respectively:

$$V_{ij}^R = w_{ij}(r_{ij}) \left[1 + \frac{Q_{ij}}{r_{ij}} \right] A_{ij} e^{-\alpha_{ij} r_{ij}} \tag{2.4}$$

$$V_{ij}^A = -w_{ij}(r_{ij}) \sum_{n=1}^{3} B_{ij}^{(n)} e^{-\beta_{ij}^{(n)} r_{ij}} \tag{2.5}$$

Here, Q is the charge, r is the atomic distance, w limits the interaction range, which is expressed as:

Table 2.2 Main function parameters of C-C bonds (AIREBO potential)

Parameters	Value	Parameters	Value
B1	12,388.79197798 eV	*Q*	0.3134602960833 Å
B2	17.56740646509 eV	*A*	10,953.544162170 eV
B3	30.71493208065 eV	α	4.7465390606595 $Å^{-1}$
$\beta 1$	4.7204523127 $Å^{-1}$	D_{min}	1.7 Å
$\beta 2$	1.4332132499 $Å^{-1}$	D_{max}	2.0 Å
$\beta 3$	1.3826912506 $Å^{-1}$		

$$w_{ij}(r_{ij}) = \begin{cases} 1 & r < D_{ij}^{\min} \\ 1 + \cos\left(\frac{r - D_{ij}^{\min}}{D_{ij}^{\max} - D_{ij}^{\min}}\right) & D_{ij}^{\min} < r < D_{ij}^{\max} \\ 0 & D_{ij}^{\max} < r \end{cases} \tag{2.6}$$

For the C-C bonds, some of the main parameters are shown in Table 2.2:

2.2.3.3 Tersoff Potential

Tersoff potential function can consider the influence of covalent bond, atomic local environment and bond angle and other factors on the bond order, so it has a good description of the formation and break of covalent bond. Tersoff potential function is widely used in the interaction between carbon and silicon materials, and can also be used to simulate the interaction of carbon-nitrogen, carbon-boron, and silicon-oxygen atoms. In this paper, the Tersoff potential function was used to describe the interaction between Si-O, C-N and C-B atoms. The potential energy function is expressed as:

$$E = \frac{1}{2}\sum_{i}\sum_{j \neq i} V_{ij} \tag{2.7}$$

$$V_{ij} = f_C(r_{ij})[f_R(r_{ij}) + b_{ij} f_A(r_{ij})] \tag{2.8}$$

In the formula (2.8), r_{ij} represents the distance between atoms, and the interaction termination function f_c can be expressed as:

$$f_C(r) = \begin{cases} 1 & : & r < R - D \\ \frac{1}{2} - \frac{1}{2}\sin\left(\frac{\pi}{2}\frac{\pi - R}{D}\right) & : & R - D < r < R + D \\ 0 & : & r > R + D \end{cases} \tag{2.9}$$

f_R describes the two-body effect:

$$f_R(r) = A\ \exp(-\lambda_1 r) \tag{2.10}$$

f_A describes the multi-body action:

$$f_A(r) = -B\ \exp(-\lambda_2 r) \tag{2.11}$$

b_{ij} is a factor that characterizes the intensity of the multibody effect, which can be expressed as:

$$b_{ij} = (1 + \beta^n \varsigma_{ij}^n)^{-\frac{1}{2n}} \tag{2.12}$$

$$\varsigma_{ij} = \sum_{k \neq i,j} f_C(r_{ik}) g(\theta_{ijk}) \exp\left[\lambda_3^m (r_{ij} - r_{ik})^m\right] \tag{2.13}$$

$$g(\theta_{ijk}) = \gamma_{ijk}\left(1 + \frac{c^2}{d^2} - \frac{c^2}{\left[d^2 + (\cos\theta - \cos\theta_0)^2\right]}\right) \tag{2.14}$$

θ_{ijk} is the bond angle between *i*-*j* and *j*-*k*, and the remaining parameter values are given in the associated potential energy function file.

2.2.3.4 ZBL Exclusion Potential

The collision force between the incident ions and the graphene was described by the collision energy (ZBL), which uses the transfer function to decay the energy and force into zero within the cut-off range. For the collision between Si, N, B atoms and C atoms in graphene, the ZBL potential function was applied based on the Tersoff potential function, and a Fermi function was adopted to smoothly connect the ZBL exclusion potential and the Tersoff potential energy at the position near the nucleus. The expression is:

$$E = \frac{1}{2} \sum_i \sum_{j \neq i} V_{ij} \tag{2.15}$$

$$V_{ij} = (1 - f_F(r_{ij})) V_{ij}^{ZBL} + f_F(r_{ij}) V_{ij}^{Tersoff} \tag{2.16}$$

where f_F is the Fermi function that connects Tersoff and ZBL potentials, which is expressed as:

$$f_F(r_{ij}) = \frac{1}{1 + e^{-A_F(r_{ij} - r_C)}} \tag{2.17}$$

In Eq. (2.17), r_C is the cutoff radius of ZBL potential. The Tersoff potential section was already described in Sect. 2.2.3.3, and the potential energy of the ZBL exclusion section can be expressed as:

$$V_{ij}^{ZBL} = \frac{1}{4\pi\varepsilon_0}\frac{Z_1 Z_2 e^2}{r_{ij}}\phi(r_{ij}/a) \tag{2.18}$$

$$a = \frac{0.8854a_0}{Z_1^{0.23} + Z_2^{0.23}} \tag{2.19}$$

$$\phi(x) = 0.1818e^{-3.2x} + 0.5099e^{-0.9423x} + 0.2802e^{-0.4029x} + 0.02817e^{-0.2016x} \tag{2.20}$$

where Z_1 and Z_2 represent the number of nucleus electrons in the collision, e is the electronic valence, ε_0 is the vacuum dielectric constant, a_0 is the Bohr radius, and the remaining coefficients were given by the original literature.

For the interaction between inert gases like argon and carbon atoms, only the ZBL exclusion potential was used.

2.2.4 Integral Algorithm

MD simulation is to discretize the motion equation in time and space, and use the finite difference equation to solve the motion state of the particles in the time domain. In this process, the time domain is discretized by a finite grid node, and the spacing of adjacent grid points is defined as the time step Δt. The basic process of the solution of MD is to bring the position and velocity of atoms at time t into the Newtonian motion equations to obtain the atomic state at time t + Δt. This process involves a large number of numerical iterations. In order to solve this problem, many different types of integration algorithms were proposed and developed, among which the Verlet algorithm is proved to have good accuracy and stability, and the calculation process is relatively simple. So it's the most widely used algorithm in MD simulation. In this paper, Verlet type algorithm was chosen to do the numerical integration.

The basic idea of the Verlet algorithm is to Taylor expand $\vec{r}_i(t+\Delta t)$ and $\vec{r}_i(t-\Delta t)$ at t:

$$\vec{r}_i(t+\Delta t) = \vec{r}_i(t) + \frac{d\vec{r}_i(t)}{dt}\Delta t + \frac{1}{2}\frac{d^2\vec{r}_i(t)}{dt^2}\Delta t^2 + \frac{1}{3!}\frac{d^3\vec{r}_i(t)}{dt^3}\Delta t^3 + O(\Delta t^4) \tag{2.21}$$

$$\overrightarrow{r}_i(t-\Delta t)=\overrightarrow{r}_i(t)-\frac{d\overrightarrow{r}_i(t)}{dt}\Delta t+\frac{1}{2}\frac{d^2\overrightarrow{r}_i(t)}{dt^2}\Delta t^2-\frac{1}{3!}\frac{d^3\overrightarrow{r}_i(t)}{dt^3}\Delta t^3+O(\Delta t^4) \tag{2.22}$$

Adding (2.21) and (2.22) together, and ignoring the higher order terms of Δt^4 and above, we can get:

$$\overrightarrow{r}_i(t+\Delta t)=2\overrightarrow{r}_i(t)-\overrightarrow{r}_i(t-\Delta t)+\frac{d^2\overrightarrow{r}_i(t)}{dt^2}\Delta t^2 \tag{2.23}$$

Subtracting (2.22) from (2.21), and ignoring the high order of Δt^3 and above, we can get:

$$\frac{d\overrightarrow{r_i}(t)}{dt}=\frac{\overrightarrow{r_i}(t+\Delta t)-\overrightarrow{r_i}(t-\Delta t)}{2\Delta t} \tag{2.24}$$

So the basic form of Verlet algorithm is:

$$\begin{cases}\overrightarrow{r}_i(t+\Delta t)=2\overrightarrow{r}_i(t)-\overrightarrow{r}_i(t-\Delta t)+\overrightarrow{a_i}(t)\Delta t^2\\ \overrightarrow{v_i}(t)=\frac{\overrightarrow{r_i}(t+\Delta t)-\overrightarrow{r_i}(t-\Delta t)}{2\Delta t}\end{cases} \tag{2.25}$$

It can be seen from function (2.25) that due to the difference in the truncation error, the calculation of the velocity in the Verlet algorithm is behind the calculation of the position. In order to obtain the position and speed at the same time, some improved Verlet integral methods were developed. The Velocity-Verlet algorithm can calculate the velocity, position and acceleration at the same time, and the calculation precision is relatively high and the calculation time is moderate. So the Velocity-Verlet algorithm is widely used, and also chosen by this paper. The basic form of the Velocity-Verlet algorithm is:

$$\begin{cases}\overrightarrow{r}_i(t+\Delta t)=\overrightarrow{r}_i(t)+\overrightarrow{v_i}(t)\Delta t+\frac{1}{2}\overrightarrow{a_i}(t)\Delta t^2\\ \overrightarrow{v_i}(t+\Delta t)=\overrightarrow{v_i}(t)+\frac{1}{2}\left(\overrightarrow{a_i}(t)+\overrightarrow{a_i}(t+\Delta t)\right)\Delta t\end{cases} \tag{2.26}$$

Verlet algorithm increases the speed of calculation by sacrificing a part of the calculation accuracy. In order to ensure the accuracy of the calculation of energy, this paper used a small time step. In the subsequent MD simulation, if there is no special illustration, the calculation time step was selected as 0.1 fs.

2.2.5 *Simulation Ensemble*

In order to more truly reflect the actual physical process, the classic MD simulation is often carried out under certain ensemble conditions. The ensemble is a collection

of independent systems that have exactly the same structure and properties and exist in a variety of motion states. The ensembles used in this paper are describes as following:

1. NVE

If the particles of the system are evolved along a constant energy orbit during the course of the movement (energy is fixed), and the particle number N and volume V of the system remain constant, then the system is in the NVE. It can be seen from the definition that NVE is isolated and conservative system.

2. NVT

NVT is the system with constant particle number N, constant temperature T and constant volume V. In order to keep the system temperature constant, a hot bath from outside can be used to coexist with the system, so that it is in thermal equilibrium condition. Also the constant temperature can be achieved by velocity scaling.

3. NPT

In the NPT, the system has a defined temperature T, pressure P and particle number N. To achieve the constant temperature, the adjustment method is the same as NVT ensemble. The adjustment of the pressure is more complex, it is often realized through the system volume scaling.

2.2.6 Averaging of Statistical Results

In this paper, MD was used to explain the phenomena of graphene irradiated by particle beams, and also describe the mechanical properties of graphene after irradiation. Therefore, in addition to the need for describing the dynamic variation of atomic structure in nano-scale, it is also needed to extract some other macro physical quantities, such as temperature field distribution of graphene structure, energy change of the system, the system stress field distribution, and so on. The following describes the extraction method of main physical quantities.

2.2.6.1 Energy

In MD, the total energy of the system contains both kinetic energy and potential energy:

$$E(t) = E_k(t) + U(t) \tag{2.27}$$

where U(t) is solved by the potential energy function described above, and the kinetic energy is calculated from the following equation:

$$E_k(t) = \left(\frac{1}{2}\sum_{i=1}^{N} m_i v_i^2(t)\right) \tag{2.28}$$

2.2.6.2 Temperature

The temperature field in the MD simulation is for a group of atoms, which is converted from the kinetic formula of the system. For a system with N particles in three-dimensional case, the kinetic energy is:

$$E_k = \frac{3N}{2} k_B T \tag{2.29}$$

By converting Eq. (2.29), the expression of the system temperature can be derived as:

$$T = \frac{2}{3Nk_B} E_k = \frac{1}{3Nk_B} \left\langle \sum_i m_i v_i^2 \right\rangle \tag{2.30}$$

2.2.6.3 Stress

In this paper, the analysis of the mechanical properties of graphene involves the extraction of single atom stress and the calculation of the stress and strain of the whole system. The extraction method of single atom stress is as follows:

$$\begin{aligned} S_{ab} = -\,[& mv_a v_b + \frac{1}{2}\sum_{n=1}^{N_p}(r_{1a}F_{1b} + r_{2a}F_{2b}) + \frac{1}{2}\sum_{n=1}^{N_b}(r_{1a}F_{1b} + r_{2a}F_{2b}) \\ & + \frac{1}{3}\sum_{n=1}^{N_a}(r_{1a}F_{1b} + r_{2a}F_{2b} + r_{3a}F_{3b}) \\ & + \frac{1}{4}\sum_{n=1}^{N_d}(r_{1a}F_{1b} + r_{2a}F_{2b} + r_{3a}F_{3b} + r_{4a}F_{4b}) \\ & + \frac{1}{4}\sum_{n=1}^{N_i}(r_{1a}F_{1b} + r_{2a}F_{2b} + r_{3a}F_{3b} + r_{4a}F_{4b}) + Kspace(r_{ia}, F_{ib}) + \sum_{n=1}^{N_f} r_{ia}F_{ib}] \end{aligned} \tag{2.31}$$

In the formula (2.31), assigning x, y, z to a, b can get the corresponding six components stress tensor, respectively. The right side of the equation corresponds to the kinetic energy, pair potential, bonding, body angle, dihedral angle, uncertain item, coulomb term, and binding term.

Note that the stress calculated in Eq. (2.31) is actually the result of the atomic stress multiplied by the volume. The true single-atom stress should be the calculated value divided by the single-atom volume, but it is impossible to calculate the volume of a single carbon atom during the tensile deformation. Therefore, the atomic stress distribution in this paper is actually the result of the stress multiplied by the volume. But it does not affect the distribution of the atomic stress, so this treatment is reasonable.

For the tensile stress of the whole system, the stress of all the atoms is summed and divided by the volume V of the system after the single-atom stress is calculated by using the formula (2.31). That is, the stress value of the system during stretching is:

$$\sigma = \frac{\sum_{i=1}^{N} S_{ab}}{V} \tag{2.32}$$

2.2.7 Introduction of Simulation Software

The MD simulation software used in this paper is LAMMPS [5], which is a parallel MD code developed by Sandia National Laboratory. LAMMPS is widely used to simulate the structure and thermodynamic properties of carbon nanomaterials. Its reliable algorithms and parallel processors ensure that the process of particle beam irradiation of graphene is truly reproduced on a computer.

2.3 Electronic Transport Theory

2.3.1 Introduction

In this paper, the electronic transport properties of graphene before and after particle beam irradiation were investigated by the methods of DFT and NEGF. In this section, the basic theorem of DFT was introduced first, and then the detail form of NEGF was described. After that, the process of solving the electronic transport properties of graphene under DFT and NEGF framework was depicted. Finally, the software for calculating the transport properties was given.

2.3.2 DFT

In the traditional quantum theory, in order to solve the electronic structure of matter, usually the electronic wave function is taken as the basic physical quantity, and then by solving the electronic Schrodinger equation, the basic physical properties are determined. For complex systems, solving the Schrodinger equation for multi-electron system is confronted with large data processing, which is impossible

to be handled accurately at present. With the development of computational materials science, there are a variety of reasonable approximations and simplifications gradually evolved. The basic idea of the modern first-principles method is firstly transferring the multi-body problem to the multi-electron system by the Born-Oppenheimer approximation, and then using the Hartree-Fock approximation and DFT theory to transfer the multi-electron system problem to the single electron system problem, for which the single electron moves in the average potential of the other nuclei and electrons.

2.3.2.1 Born-Oppenheimer and Hartree-Fock Approximation

To solve the electronic energy level of the solid system, we need to solve the Schrodinger equation:

$$H(\overrightarrow{r}, \overrightarrow{R})\Psi(\overrightarrow{r}, \overrightarrow{R}) = E\Psi(\overrightarrow{r}, \overrightarrow{R}) \tag{2.33}$$

where E and Ψ are the energy eigenvalues and wave functions describing the system, H is the Hamiltonian of the system, and $\overrightarrow{r}$ and $\overrightarrow{R}$ is the set of coordinates for all the electrons and nuclei in the system, respectively. If the influence of the external field is neglected, the H of the system is expressed as several items: the electron kinetic energy and the coulomb potential energy induced by the interaction between different electrons, the nucleus kinetic energy and the coulomb potential energy induced by the interactions between nucleuses, the interaction between the electron and the nucleus:

$$\begin{aligned} H(\overrightarrow{r}, \overrightarrow{R}) = &-\sum_i \frac{\hbar^2}{2m}\nabla_{r_i}^2 + \frac{1}{2}\sum_{ii'} \frac{e^2}{\left|\overrightarrow{r_i} - \overrightarrow{r_{i'}}\right|} \\ &-\sum_j \frac{\hbar^2}{2M_j}\nabla_{R_j}^2 + \frac{1}{2}\sum_{jj'} V_n(\overrightarrow{R_j} - \overrightarrow{R_{j'}}) - \sum_{ij} V_{e-n}(\overrightarrow{r_i} - \overrightarrow{R_j}) \end{aligned} \tag{2.34}$$

It is very difficult to solve the equations of electron and atomic nucleus of the multi-body system. Born-Oppenheimer approximation refers to the separation of electrons and nuclei in the consideration of multibody problems, that is, when studying the electron motion, the nuclei is regarded as static potential disturbance, and when studying the movement of nuclei, neglecting the distribution of electron in space. So that electron and nuclei only need to meet their respective motion equations. Under adiabatic approximation, the Hamiltonian of the electronic part is:

$$H(\overrightarrow{r}, \overrightarrow{R}) = -\sum_i \frac{\hbar^2}{2m}\nabla_{r_i}^2 + \frac{1}{2}\sum_{ii'} \frac{e^2}{\left|\overrightarrow{r_i} - \overrightarrow{r_{i'}}\right|} - \sum_{ij} V_{e-n}(\overrightarrow{r_i} - \overrightarrow{R_j}) \tag{2.35}$$

As the weight and speed of movement of electron and atomic nucleus are largely different, reasonable results can be obtained by considering the movement of nucleus and electronic separately. The adiabatic approximation can transform the multi-body solution system into a multi-electron system. But solving of the equation of multi-electron system requires the Coulomb interaction term between electrons, which cannot be accurately determined. Hartree proposed to simplify the interaction between electrons as a single electron in the average potential field of other electrons (single electron approximation). Through this approximation, the motion state of multi-electron system is described with a single electron wave function, and multi-electron system wave function is taken as the product of the single electron wave function. Subsequently, Fock proposed to change the product of the wave function into a Slater determinant in consideration of the spin state. Finally, the single-electron equation of the system is:

$$E_i\Psi_i(\vec{r}) = \left[-\frac{\hbar^2}{2m}\nabla^2 - \sum_j V_{e-n}(\vec{R_j})\right]\Psi_i(\vec{r}) + \sum_{i'\neq i}\int d\vec{r'}\frac{\left|\Psi_{i'}(\vec{r'})\right|^2}{\left|\vec{r_i} - \vec{r_{i'}}\right|}\Psi_i(\vec{r}) + \sum_{i'\neq i}\int dr'\frac{\Psi^*_{i'}\Psi_i(\vec{r'})}{\left|\vec{r_i} - \vec{r_{i'}}\right|}\Psi_{i'}(\vec{r}) \tag{2.36}$$

The single electron wave function is obtained by solving the single electron equation, and then the multi-electron wave function of the system is obtained by the single electron wave function. Finally, the Schrodinger equation of the multi-body system is simplified as a single electron problem by the adiabatic and Hartree-Fock approximation.

2.3.2.2 Thomas-Fermi Model

As early as 1927, Thomas and Fermi proposed the Thomas-Fermi model based on homogeneous electron gas to solve the Schrodinger equation. In this model, the influence of external force on electrons, and the interaction between electrons were ignored. The total energy of the electronic system can be expressed by electron density:

$$E_{TF}[\rho(\vec{r})] = C_{TF}\int \rho(\vec{r})_{5/3}d\vec{r} - z\int\frac{\rho(\vec{r})}{\vec{r}}d\vec{r} + \frac{1}{2}\int\int\frac{\rho(\vec{r_1}) - \rho(\vec{r}_2)}{\left|\vec{r_1} - \vec{r}_2\right|}d\vec{r}_1 d\vec{r}_2 \tag{2.37}$$

Equation (2.37) shows that the energy functional of the system can be expressed as a function determined only by the electron density. In order to consider the

influence of the exchange correlation between electrons which was ignored by Thomas-Fermi model, Dirac proposed to add a geometric correction term in the formula (2.37), which is the so-called Thomas-Fermi-Dirac model:

$$E_{TF}[\rho(\overrightarrow{r})] = C_1 \int d^3\overrightarrow{r}\rho^{\frac{5}{3}}(\overrightarrow{r}) + \int d^3\overrightarrow{r}V_{ext}(\overrightarrow{r})\rho(\overrightarrow{r}) + C_2 \int d^3\overrightarrow{r}\rho^{\frac{4}{3}}(\overrightarrow{r}) + \frac{1}{2}\int d^3\overrightarrow{r}d^3\overrightarrow{r'}\frac{\rho(\overrightarrow{r})\rho(\overrightarrow{r}')}{\left|\overrightarrow{r} - \overrightarrow{r}'\right|} \tag{2.38}$$

2.3.2.3 Hohenberg-Kohn Theorem

According to the above Thomas-Fermi-Dirac model, Hohenberg and Kohn established the DFT. Strict DFT is based on two important theorems. Among them, Hohenberg-Kohn's first theorem states that the ground state energy of the system is a unique function determined only by the electron density function. It pointed out that the ground state energy of the multi-electron system and the related physical quantities and properties can be uniquely determined by the ground state electron density. The work of solving the Hamiltonian is greatly simplified by introducing the charge density function. Hohenberg-Kohn's second theorem stated that the ground state energy can be obtained by the process of minimizing the system energy based on the ground state electron density. Variation of the system energy based on electron density can determine the ground state energy, so as to obtain the other relevant physical quantities.

Under the two theorems of Hohenberg-Kohn, the energy of the system can be expressed as:

$$E[\rho] = \int d\overrightarrow{r}V_{ext}(\overrightarrow{r})d\overrightarrow{r} + F[\rho] \tag{2.39}$$

To solve the ground state energy is to find the variation of $F[\rho]$, which can be represented by kinetic energy, Coulomb term, and the exchange correlation items in the form of expression:

$$F[\rho] = T[\rho] + \frac{1}{2}\int\int d\overrightarrow{r}d\overrightarrow{r}'\frac{\rho(\overrightarrow{r})\rho(\overrightarrow{r'})}{\left|\overrightarrow{r} - \overrightarrow{r}'\right|} + E_{xc}[\rho] \tag{2.40}$$

Therefore, according to the Hohenberg-Kohn theorem, through taking the electron density of the system as the basic variable, the physical properties of the system in ground state can be solved by making the energy functional variation based on the electron density. From Eq. (2.40), it is necessary to determine three problems in order to solve the ground state energy of the system: Determining the electronic density function $\rho(\overrightarrow{r})$ of the system, determining the kinetic energy functional $T[\rho]$ of the system, and determining the exchange-correlation functional $E_{xc}[\rho]$.

2.3.2.4 Kohn-Sham Model

Under the framework of Hohenberg-Kohn theory, making the energy functional variance of the system can get:

$$\int d\vec{r}\,\delta\rho(\vec{r})\left[\frac{\delta T[\rho(\vec{r})]}{\delta\rho(\vec{r})}+V(\vec{r})+\int d\vec{r}'\frac{\rho(\vec{r}')}{\left|\vec{r}-\vec{r}'\right|}+\frac{\delta E_{xc}[\rho(\vec{r})]}{\delta\rho(\vec{r})}\right]=0 \tag{2.41}$$

Under $\int d\vec{r}\,\delta\rho(\vec{r})=0$, we can get:

$$\frac{\delta T[\rho(\vec{r})]}{\delta\rho(\vec{r})}+V(\vec{r})+\int d\vec{r}'\frac{\rho(\vec{r}')}{\left|\vec{r}-\vec{r}'\right|}+\frac{\delta E_{xc}[\rho(\vec{r})]}{\delta\rho(\vec{r})}=\mu \tag{2.42}$$

In the effective potential field, the above equation can be expressed as:

$$V_{eff}(\vec{r})=V(\vec{r})+\int d\vec{r}'\frac{\rho(\vec{r}')}{\left|\vec{r}-\vec{r}'\right|}+\frac{\delta E_{xc}[\rho(\vec{r})]}{\delta\rho(\vec{r})} \tag{2.43}$$

Due to the kinetic energy function $T[\rho]$ is unknown, in order to solve Eq. (2.41), Kohn-Sham proposed to replace $T[\rho]$ by a kinetic energy functional without considering the interaction term $T_s[\rho]$. The difference between them is considered in exchange-correlation functional. For which, the electronic density function $\rho(\vec{r})$ is solved by a single electron wave function:

$$\rho(\vec{r})=\sum_{i=1}^{N}\left|\Psi_i(\vec{r})\right|^2 \tag{2.44}$$

Thus the Kohn-Sham equation is obtained:

$$\left\{-\nabla^2+V_{ks}[\rho(\vec{r})]\right\}\Psi_i(\vec{r})=E_i\Psi_i(\vec{r}) \tag{2.45}$$

$$\begin{aligned}V_{ks}[\rho(\vec{r})]&=V(\vec{r})+V_{coul}[\rho(\vec{r})]+V_{xc}[\rho(\vec{r})]\\&=V(\vec{r})+\int d\vec{r}'\frac{\rho(\vec{r}')}{\left|\vec{r}-\vec{r}'\right|}+\frac{\delta E_{xc}[\rho(\vec{r})]}{\delta\rho(\vec{r})}\end{aligned} \tag{2.46}$$

For the above equation, the first term is the atomic nucleus attracting potential, the second term is the electron-electron interaction Coulomb term, and the third term is the exchange-correlation part. By solving the single-electron equation, the ground state performance of the system can be obtained.

2.3.2.5 Exchange-Correlation Functional

A large number of unknown parts of the Kohn-Sham equation are assigned to the exchange-correlation part. After determining the electronic density $\rho(\overrightarrow{r})$ and kinetic energy $T[\rho]$ of the system, the specific form of the exchange-correlation part must be obtained. There are different methods proposed to deal with the exchange-correlation part, among which LDA and GGA are mostly used. The basic idea of LDA is to use the density function of more uniform electron gas to get the exchange-correlation form of non-uniform electron gas, which is suitable for the system with slow change of electron density. GGA is more applicable for a system with large nonuniformity of the electron density or nonuniformity of the electron density plays an important role to the results. GGA is a functional considering the exchange-correlation energy as the electron charge density and its gradient. It has greatly improved the results of atomic exchange and correlation energy for many systems. However, the GGA method cannot obtain the accurate results for all systems, and the GGA method greatly increases the computational complexity. Therefore, in the actual process it is needed to select the appropriate methods based on system studied and the problems concerned.

2.3.3 Green Function Theory

Usually all the properties of the quantum mechanics system are based on the Hamiltonian of the system, and the eigenfunctions and eigenvalues of the Hamiltonian system are obtained by solving the Schrodinger equation. The solution of Schrodinger equation needs to theoretically construct the wave function. While the solving of the wave function of an actual complex system is impossible, this makes people continually seek new methods and theories to get rid of the solution of wave function to get the system ground state energy, eigenvalue and other physical quantities. Green function method is to describe the system from the particle movement, to avoid solving the wave function to get the relevant physical properties. The physical quantities obtained by solving the Hamiltonian can also be obtained by solving the Green's function. According to the different processing systems, Green's function is divided into equilibrium Green's function and NEGF.

2.3.3.1 NEGF

The equilibrium Green function is defined on the real time axis, and the NEGF is defined on the contour of the complex time plane. The contour-ordered Green function defined in the complex time plane is:

$$G^C(1,1') \equiv -i\left\langle T_C\psi(1)\psi^\dagger(1')\right\rangle \tag{2.47}$$

where $(1) \equiv (r_1, t_1)$ and $(1') \equiv (r_{1'}, t_{1'})$ are abbreviations of the spatial and temporal variables, respectively. The line C starts from $-\infty$ and ends with ∞, passing through the real time axis at time t_0. The upper and lower paths of the real time axis are labeled as C_1 and C_2, respectively. T_C is a complex weave operator defined on the contour. For two-time scale on the contour, defining the following Green function:

$$G^C(1,1') \equiv \begin{cases} G^t(1,1') & t_1, t_{1'} \in C_1 \\ G^>(1,1') & t_1 \in C_1, t_{1'} \in C_2 \\ G^<(1,1') & t_1 \in C_2, t_{1'} \in C_1 \\ \tilde{G^t}(1,1') & t_1, t_{1'} \in C_2 \end{cases} \tag{2.48}$$

Among them, the time series Green function $G^t(1,1')$, greater Green function $G^>(1,1')$, less Green function $G^<(1,1')$, anti-temporal Green function $G^{\tilde{t}}(1,1')$, retarding Green function $G^R(1,1')$, advancing Green function $G^A(1,1')$ are written as:

$$G^t(1,1') \equiv -i\theta(t_1 - t_{1'})\left\langle\psi(1)\psi^\dagger(1')\right\rangle + i\theta(t_{1'} - t_1)\left\langle\psi^\dagger(1')\psi(1)\right\rangle \tag{2.49}$$

$$G^>(1,1') \equiv -i\left\langle\psi(1)\psi^\dagger(1')\right\rangle \tag{2.50}$$

$$G^<(1,1') \equiv -i\left\langle\psi^\dagger(1')\psi(1)\right\rangle \tag{2.51}$$

$$G^{\tilde{t}}(1,1') \equiv -i\theta(t_{1'} - t_1)\left\langle\psi(1)\psi^\dagger(1')\right\rangle + i\theta(t_1 - t_{1'})\left\langle\psi^\dagger(1')\psi(1)\right\rangle \tag{2.52}$$

$$G^R(1,1') = \theta(t_1 - t_{1'})[G^>(1,1') - G^<(1,1')] \tag{2.53}$$

$$G^A(1,1') = \theta(t_{1'} - t_1)[G^<(1,1') - G^>(1,1')] \tag{2.54}$$

The six Green functions are related to each other. In order to solve the non-equilibrium state, only four Green functions need to be known. Among them, the retarding and the advancing Green function describe the energy spectrum, the state density, etc. The greater and less Green functions describe the particle number information in the system.

The Dyson equation can consider the self-energy, the Green's function and the undisturbed Green's function all together. The Dyson equation is:

$$G^C(1,1') = G_0^C(1,1') + \int dx_2 \int_C d\tau_2 G_0^C(1,2)U(2)G^C(2,1') + \int dx_2 \int dx_3 \int_C d\tau_2 \int_C d\tau_3 G_0^C(1,2)\sum{}^C(2,3)G^C(3,1') \tag{2.55}$$

In the Dyson equation, $G_0^C(1,1')$ is the Green function of a system without any interactions. The external potential energy U includes the non-equilibrium part. Self-energy $\sum^C[G]$ has the interaction part. Therefore, it describes the method of using the non-interaction Green's function to represent the system with interaction.

In solving the non-equilibrium system, Keldysh also proposed the corresponding motion equations:

$$G^R = G_0^R + G_0^R \sum{}^R G^R \tag{2.56}$$

$$G^A = G_0^A + G_0^A \sum{}^A G^A \tag{2.57}$$

$$G^< = (1 + G^R \sum{}^R) + G_0^< (1 + G^A \sum{}^A) + G^R \sum{}^< G^A \tag{2.58}$$

$$G^> = (1 + G^R \sum{}^R) + G_0^> (1 + G^A \sum{}^A) + G^R \sum{}^> G^A \tag{2.59}$$

$$G^t = (1 + G^R \sum{}^R) + G_0^t (1 + G^A \sum{}^A) + G^R \sum{}^t G^A \tag{2.60}$$

$$G^{\tilde{t}} = (1 + G^R \sum{}^R) + G_0^{\tilde{t}} (1 + G^A \sum{}^A) + G^R \sum{}^{\tilde{t}} G^A \tag{2.61}$$

2.3.3.2 NEGF Theory in Electronic Transport

By using the NEGF method, the electron density matrix of the system can be obtained without solving the wave function, which provides an effective method for studying the electronic transport properties of the non-equilibrium open system.

In a system described by Hamiltonian, the Green function is defined as:

$$G(z) = (z\hat{S} - \hat{H})^{-1} \tag{2.62}$$

where z is defined on the complex plane and $\hat{S}$ is the overlapping matrix of the base set. In the study of electronic transport problems, the solution of such systems corresponds to infinite $\hat{H}$ and $\hat{S}$, and the corresponding matrix $(z\hat{S} - \hat{H})$ is also bound to be infinite, so we are facing a problem of solving the inversion of infinite matrix. But in fact, it is possible to obtain the properties of the whole system only

by solving the Green function of the intermediate scattering part through shield approximation.

The matrix $(z\hat{S} - \hat{H})$ can be written according to the left and right electrodes and the scattering section:

$$z\hat{S} - \hat{H} = \begin{bmatrix} z\hat{S}_L - \hat{H}_L & \tau_L & 0 \\ \tau'_L & z\hat{S}_d - \hat{H}_d & \tau'_R \\ 0 & \tau_R & z\hat{S}_R - \hat{H}_R \end{bmatrix} \tag{2.63}$$

where L and R denote left and right electrodes, d denotes an intermediate scattering region. $\tau_i = z\hat{S}_{id} - \hat{H}_{id}$ and $\tau'_i = z\hat{S}_{di} - \hat{H}_{di}$ represent the interaction between an electrode and an intermediate scattering region, respectively. While the interaction between the two electrodes can be simplified to zero. For the solution of the Green function G, it can be expressed in block form:

$$\begin{bmatrix} z\hat{S}_L - \hat{H}_L & \tau_L & 0 \\ \tau'_L & z\hat{S}_d - \hat{H}_d & \tau'_R \\ 0 & \tau_R & z\hat{S}_R - \hat{H}_R \end{bmatrix} \begin{bmatrix} G_L & G_{Ld} & G_{LR} \\ G_{dL} & G_d & G_{dR} \\ G_{RL} & G_{Rd} & G_R \end{bmatrix} = I \tag{2.64}$$

From which, G_d can be obtained as:

$$G_d = (z\hat{S}_d - \hat{H}_d - \sum{}_L(z) - \sum{}_R(z))^{-1} \tag{2.65}$$

In which, $\sum{}_i(z)$ is the self-energy of the system:

$$\sum{}_i(z) = \tau'_i g_i(z) \tau_i \tag{2.66}$$

The electrode Green function $g_i(z)$ is expressed as:

$$g_i(z) = (z\hat{S} - \hat{H}_i)^{-1} \tag{2.67}$$

The density of States in the intermediate extended region can be obtained directly from the spectral function:

$$DOS(E) = \frac{1}{2\pi} Tr\left[A(E)\hat{S}\right] = \sum_n \delta(E - E_n) \tag{2.68}$$

Under the equilibrium state, the density matrix can be obtained by integrating the spectral function below the Fermi level. In the case of external bias, the electronic state and density matrices are divided into an equilibrium part and a non-equilibrium part, where the electronic state below the lowest Fermi level μ_R constitutes the density matrix of the equilibrium part, which is expressed as:

$$\rho^{eq} = \frac{1}{2\pi}\int_{E_{\min}}^{\mu_R} A(E)dE = \frac{i}{2\pi}\int_{E_{\min}}^{\mu_R} (G^R(E) - G^A(E))dE \tag{2.69}$$

The electronic states between μ_R and μ_L forms a non-equilibrium density matrix. The density matrix of the non-equilibrium part can be obtained by integrating the left spectrum function:

$$\rho^{ne} = \frac{1}{2\pi}\int_{\mu_R}^{\mu_L} A(E)dE = \frac{i}{2\pi}\int_{\mu_R}^{\mu_L} (G^R[\Gamma_L f(E-\mu_L)]G^A dE \tag{2.70}$$

$\Gamma_L = i(\sum_L - \sum_L^+)$ is the imaginary part of the self-energy of left electrode.

Therefore, the density matrix of the system can be firstly obtained by the NEGF method, and then the other electronic structure properties of the system can be derived. Finally, the electronic transport current of the system can be obtained by Landauer-Büttiker formula:

$$I = \frac{2e}{h}\int [f(E-\mu_L) - f(E-\mu_R)]T(E,V)dE \tag{2.71}$$

$T(E,V) = Tr\left[\Gamma_L G_d^{R^*}\Gamma_R G_d^R\right]$ is the transmission function.

2.3.4 *Solution Process of the Electronic Transport Properties of Graphene*

In order to solve the electronic transport properties of graphene before and after particle beam irradiation, this thesis adopted the method combining DFT and NEGF theory. The specific solving process is as follows:

1. First, the non-equilibrium system to be solved is divided into three parts, in which the left and right parts are semi-infinite electrode region, and the middle part is the scattering area, as shown in Fig. 2.4. This double electrode model can be used to simulate the contact between the electrode region and the scattering region and the carriers transport process in the intermediate scattering region in actual measurement.
2. Solving the transmission of the system by means of the Green's function using the self-consistent process as shown in Fig. 2.5, and then using the Landauer-Büttiker (Eq. 2.71) to solve the current value between the left and right electrodes.

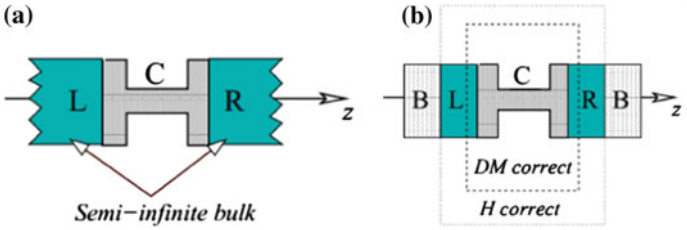


Fig. 2.4 Two-electrode model for calculation of the transport properties of graphene. Reprinted with permission from Ref. [6], Copyright 1998 by American Physical Society

2.3.5 Introduction to Simulation Software

This paper calculated the transport properties of graphene using Transiesta software [6], which combines DFT theory with NEGF theory. It is an open source code developed on the basis of SIESTA software. The non-local conservation pseudopotential was used to describe nuclear electrons and the valence electrons were described by atomic orbital linear combination in finite regions. Combining NEGF method, the electronic transport properties of semi-infinite long electrode molecular devices can be self-consistently calculated, especially under different bias conditions. At present, the commercial software ATK (Atomistix ToolKit) [7] developed based on it has already been widely used in the calculation of the electronic transport properties of CNTs, graphene and other carbon materials. The Transiesta software is very suitable for studying the electronic transport properties of systems with graphene doping, joining and nanoporous structure.

2.4 Chapter Summary

This chapter introduced the experimental and simulation methods used in this research, including the preparation and transfer of graphene materials and the methods of graphene processing and detection. It also included the basic theory of MD simulation and electronic transport calculation. The experiment and the simulation methods used in the subsequent chapters were based on the contents of this chapter, so similar contents in the subsequent sections will not be repeated.

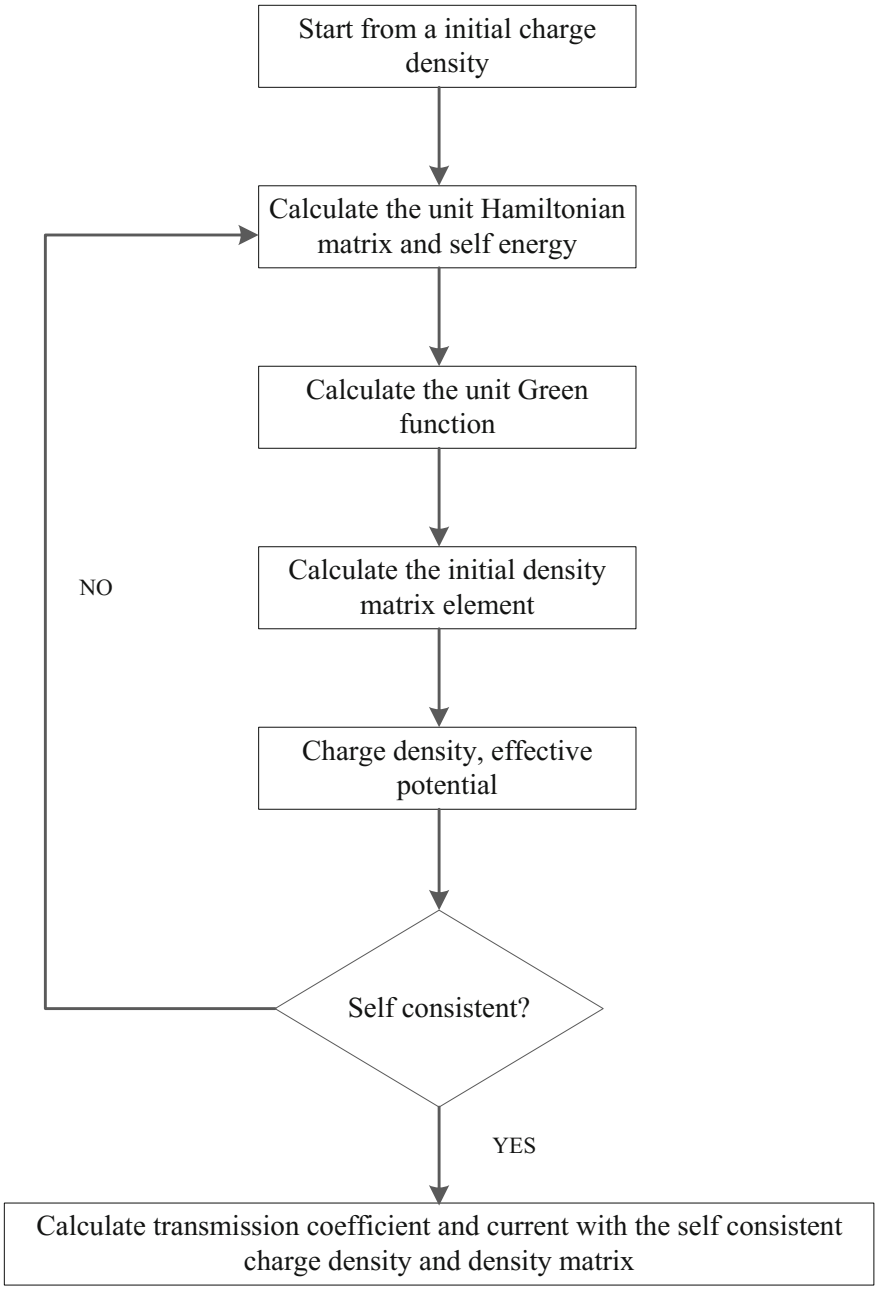


Fig. 2.5 Solution procedure of electron transport properties (DFT + NEGF method)

References

1. Ferrari AC, Meyer JC, Scardaci V et al (2006) Raman spectrum of graphene and graphene layers. Phys Rev Lett 97:187401
2. Stuart SJ, Tutein AB, Harrison JA (2000) A reactive potential for hydrocarbons with intermolecular interactions. J Chem Phys 112:6472–6486
3. Ziegler JF, Biersack JP, Littmark U (1985) The stopping and range of ions in matter. Pergamon, New York
4. Tersoff J (1988) New empirical approach for the structure and energy of covalent systems. Phys Rev B 37:6991
5. Plimpton S (1995) Fast parallel algorithms for short-range molecular dynamcis. J Comput Phys 117:1–19
6. Brandbyge M, Mozos JL, Ordejon P et al (2002) Density-functional method for nonequilibrium electron transport. Phys Rev B 65:165401
7. www.atomistix.com

http://www.springer.com/978-981-10-6456-2

Influence of Particle Beam Irradiation on the Structure and Properties of Graphene

Wu, X.

2018, XV, 182 p. 125 illus., 115 illus. in color.,
Hardcover
ISBN: 978-981-10-6456-2